Effect of pseudogap on electronic anisotropy in the strain dependence of the superconducting Tc of underdoped YBa2Cu3Oy

M. Frachet, D. J. Campbell, A. Missiaen, S. Benhabib, F. Laliberté, B. Borgnic, T. Loew, J. Porras, S. Nakata, B. Keimer, et al.

Evidence for interplay between pseudogap and orthorhombicity in underdoped $YBa_2Cu_3O_y$ from ultrasound measurements

M. Frachet,[1,*] Daniel J. Campbell,[1] Anne Missiaen,[1] S. Benhabib,[1] Francis Laliberté,[1] B. Borgnic,[1] T. Loew,[2] J. Porras,[2] S. Nakata,[2] B. Keimer,[2] M. Le Tacon,[3] Cyril Proust,[1] I. Paul,[4,†] and David LeBoeuf[1,‡]

[1] *LNCMI-EMFL, CNRS UPR3228, Univ. Grenoble Alpes, Univ. Toulouse, Univ. Toulouse 3, INSA-T, Grenoble and Toulouse, France*

[2] *Max-Planck-Institut für Festkörperforschung, Heisenbergstrasse 1, Stuttgart, D-70569, Germany*

[3] *Institute for Quantum Materials and Technologies, Karlsruhe Institute of Technology, D-76344, Eggenstein-Leopoldshafen, Germany*

[4] *Laboratoire Matériaux et Phénomènes Quantiques, CNRS, Université de Paris, F-75205 Paris, France*

(Dated: June 2, 2021)

Using ultrasound measurements on detwinned single crystals of underdoped $YBa_2Cu_3O_y$ (YBCO) we study the hole doping (p) evolution of the thermodynamic anisotropy obtained by comparing the strain dependence of superconducting T_c along the a and b crystallographic directions. While the structural orthorhombicity of YBCO reduces monotonically with decreasing $p < 0.16$, we find that the thermodynamic anisotropy shows an intriguing enhancement at intermediate doping level of electronic origin. Our theoretical analysis shows that the enhancement of the electronic anisotropy can be related to the pseudogap potential that itself increases when the Mott insulating state is approached. Our results imply that the pseudogap is controlled by a local energy scale that can be tuned by varying the nearest neighbor Cu-Cu bond length. Our work opens the possibility to strain engineer the pseudogap potential to enhance the superconducting T_c.

The link between electronic anisotropy and high temperature superconductivity in the cuprates and the iron based systems is a subject of great current interest. While a lot of progress on this topic has been made for the iron based systems, relatively less is known about the in-plane electronic anisotropy observed in the pseudogap state of certain underdoped cuprates [1–12]. The microscopic factors governing this anisotropy are currently unknown, and are the subject of intense research [13–18]. Evidently, identifying the source of this anisotropy is of utmost importance for understanding the pseudogap state and the phase diagram of the cuprates. The purpose of the current joint experimental and theoretical study is to address this issue.

Experimentally, the anisotropy has been probed using a variety of techniques including in-plane electrical conductivity [1], torque magnetometry [2], neutron [3, 4] and X-ray [5] diffraction, Nernst coefficient [6, 7], scanning tunneling spectroscopy [8, 9], nuclear magnetic resonance [10], and elastoresistivity [11]. One school of thought has identified the pseudogap temperature $T^\star$ with an electronic nematic phase transition [2]. However, the situation is unclear because signatures of diverging nematic correlation, expected near a nematic phase transition [19], have not been detected in electronic Raman response in $Bi_2Sr_2CaCu_2O_{8+\delta}$ [20].

Motivated by the status quo, we study the doping evolution of the thermodynamic anisotropy $N \equiv dT_c/d\epsilon_{22} - dT_c/d\epsilon_{11}$, where $dT_c/d\epsilon_{ii}$ is the variation of the superconducting T_c with uniaxial strain ϵ_{ii}, $ii = (11, 22)$, of underdoped $YBa_2Cu_3O_y$ (YBCO). The experimental technique involves measuring the jumps in the associated elastic constants Δc_{ii} at T_c using sound velocity measurements (see Fig. 1), from which we extract $dT_c/d\epsilon_{ii}$ using the Ehrenfest relationship. The advantage of this method is that the strain dependence of T_c is obtained in *zero* applied static strain. Consequently, the measurement is free of nonlinear effects that can be difficult to interpret. To the best of our knowledge, such strain dependence of T_c has not been reported earlier in YBCO. This thermodynamic anisotropy is in line with earlier studies of uniaxial pressure dependencies of T_c [21, 22]. However, converting them into strain dependencies is difficult due to the large uncertainties in the experimental values of the elastic constant tensor.

Our main observation is that, while the crystalline anisotropy, namely the orthorhombicity, reduces monotonically with decreasing hole doping $p < 0.16$ [23–25], the thermodynamic anisotropy $N(p)$ is a non monotonic function of p (see Fig. 2). In particular, in the range $0.11 < p < 0.14$, $N(p)$ does not track the orthorhombicity, instead it increases when p is reduced. We therefore conclude that the observed non-monotonic evolution is rooted in electronic effects. Our theoretical modeling suggests that the enhanced electronic anisotropy in this doping range is driven by the opening of the pseudogap. In other words, the increase in anisotropy with decreasing doping level reflects the fact that the pseudogap potential enhances as the system approaches the Mott insulating state by reducing p.

The sound velocities of several detwinned YBCO sam-

* Present adress: Institute for Quantum Materials and Technologies, Karlsruhe Institute of Technology, D-76344, Eggenstein-Leopoldshafen, Germany

† indranil.paul@univ-paris-diderot.fr

‡ david.leboeuf@lncmi.cnrs.fr

y	T_c (K)	p (holes/Cu)	$dT_c/d\epsilon_{11}$(K)	$dT_c/d\epsilon_{22}$(K)
6.45	34.0	0.071	0 ± 50	0 ± 50
6.48	55.8	0.095	-	380 ± 52
6.51	60.0	0.106	0 ± 50	440 ± 70
6.55	62.5	0.113	0 ± 50	480 ± 76
6.67	67.7	0.122	475 ± 85	720 ± 115
6.75	77.0	0.134	655 ± 135	845 ± 175
6.79	82.0	0.138	450 ± 102	560 ± 100
6.87	92.3	0.156	0 ± 50	400 ± 65
6.99	88.5	0.185	-	320 ± 34

TABLE I: Characteristics of the YBCO samples measured in this study: the oxygen content y; the superconducting transition temperature in zero magnetic field T_c; the hole concentration (doping) p, obtained from T_c [26]. Typical $dT_c/d\epsilon_{11}$ and $dT_c/d\epsilon_{22}$ are given for each oxygen content y.

ples (see Table I for characteristics) measured across their superconducting transition temperature T_c are shown in Fig. 1 (see [27] for experimental details and additional data). We focus on the elastic constants c_{11} and c_{22} corresponding to longitudinal modes with propagation along the a-axis and b-axis of the orthorhombic crystal structure of YBCO, respectively.

In Fig. 1 we show the superconducting contribution to the elastic constants, obtained after subtraction of the thermally activated anharmonic background [28]. The latter consists of a change of slope and curvature below T_c and a downward, mean-field jump $\Delta c_{ii}(T_c)$ at T_c. This jump is a consequence of having a term $\phi^2\epsilon_{ii}$ in the free energy that couples the strain with the superconducting order parameter ϕ. Here we focus on the magnitude of this jump $\Delta c_{ii}(T_c)$, which strongly depends on doping level and on propagation direction. In particular, an anisotropy is observed between $\Delta c_{11}(T_c)$ and $\Delta c_{22}(T_c)$ at $p \leq 0.11$ and $p \geq 0.156$: at $T = T_c$, a clear jump is observed in $\Delta c_{22}(T)$ but no jump is observed in $\Delta c_{11}(T)$. However, at intermediate doping level the anisotropy is reduced, with a clear jump resolved in both modes. The magnitude of $\Delta c_{ii}(T_c)$ is governed by the Ehrenfest relationship

$$\Delta c_{ii}(T_c) = -\frac{\Delta C_p(T_c)}{T_c}\frac{1}{V_m}\left(\frac{dT_c}{d\epsilon_{ii}}\right)^2, \qquad (1)$$

with $\Delta C_p(T_c)$ the jump in the heat capacity at T_c, and V_m the molar volume [29, 30]. Thus, the anisotropy in Δc_{ii} implies a difference between $dT_c/d\epsilon_{11}$ and $dT_c/d\epsilon_{22}$.

We use a thermodynamic model to fit the data in Fig. 1 and to extract $\Delta c_{ii}(T_c)$ [27, 31]. We then use Eq. 1, in combination with specific heat [32–36] and uniaxial pressure dependence of T_c data [21, 37–42] in order to determine the amplitude and sign of $dT_c/d\epsilon_{ii}$ respectively.

The resulting doping dependencies of $dT_c/d\epsilon_{11}$ and $dT_c/d\epsilon_{22}$ are shown in Fig. 2b and the values are reported in Table I. While both quantities show a maximum

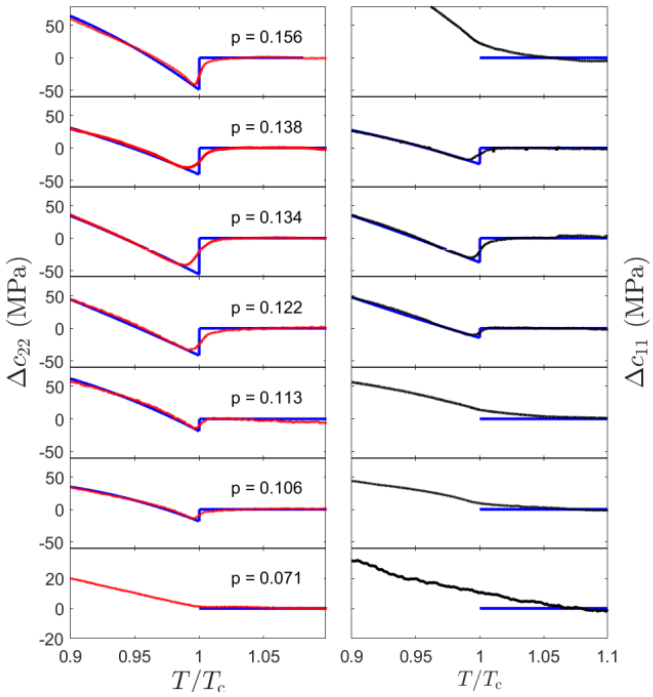

FIG. 1: Superconducting contribution to $c_{22}(T)$ (red, left column) and $c_{11}(T)$ (black, right column) near T_c as a function of doping in YBCO. A fit based on a thermodynamic model [27] is shown in blue. It is used to extract $\Delta c_{ii}(T_c)$, the mean-field jump-like anomaly at T_c. When no jump is observed we can extract an upper limit for $dT_c/d\epsilon_{ii}$ which depends on measurement noise level and on the amplitude of the specific heat jump at T_c. T_c is defined as the position of the mean-field anomaly in $\Delta c_{ii}(T)$. The scale is the same for all doping levels except for $p = 0.071$ where the vertical scale is reduced for clarity.

around $p \sim 0.13$, a doping-dependent anisotropy is observed. To make it clear, the thermodynamic anisotropy $N = dT_c/d\epsilon_{22} - dT_c/d\epsilon_{11}$ is plotted in Fig. 2c. Upon decreasing the doping level, N first decreases and features a minimum for $p \sim 0.14$. Then N rises and show a maximum at $p \sim 0.11$, where $dT_c/d\epsilon_{22}$ is at least an order of magnitude larger than $|dT_c/d\epsilon_{11}| \leq 50$ K. Finally for $p < 0.11$, N decreases steadily as a mean-field jump is no longer resolved neither in c_{11} nor in c_{22} at $p = 0.071$. Thus, $N(p)$ is non-monotonic as a function of doping, which is the main experimental result of this article.

The behavior of $N(p)$ is to be contrasted with the monotonic increase of the orthorhombicity of YBCO with doping over similar range (see [23–25] and Fig. 4 in [27]). This difference in the doping trends imply that $N(p)$ is affected by an electronic property which we try to identify in the rest of the paper. Below we discuss three possible electronic scenarios.

One possible source of additional electronic anisotropy can be the short range charge density wave (CDW) order in YBCO [10, 43, 44]. At face value this seems to

be the case since $dT_c/d\epsilon_{22}$ and $dT_c/d\epsilon_{11}$ are individually peaked around $p = 0.13$, which coincides with the peak in the CDW ordering temperature. However, this simply implies that the CDW contributes significantly in the symmetric channel $dT_c/d\epsilon_{22}+dT_c/d\epsilon_{11}$, which is likely due to a competition between CDW and superconductivity [45–48]. But, in the asymmetric channel $dT_c/d\epsilon_{22}-dT_c/d\epsilon_{11}$ we do not expect the CDW to be important for the following reason. The CDW state itself is either a biaxial order that preserves tetragonal symmetry [49], in which case it does not contribute to $N(p)$, or it is locally uniaxial with CDW domains running along the in-plane crystallographic axes as seen by X-ray [48, 50]. However, even for the latter, the CDW will contribute to $N(p)$ only if these domains are aligned along the same direction, which is not the case in the zero strain limit probed here.

A second possible explanation could be the presence of a significantly large B_{1g} nematic correlation length, that presumably increases as the doping level p is reduced. However, in such a case one would expect in theory that the magnitude of the elastic constant jumps $\Delta c_{ii}/c_{ii}$ to be orders of magnitude larger than their typical value 10^{-5} measured in our experiments [51]. Consistently, a dynamical mean field study has reported lack of any significant nematic correlations [18].

The third possibility, which we explore in detail, is that $N(p)$ is governed by the opening of the pseudogap in the single particle electronic properties. This is based on the hypothesis that the pseudogap potential varies with external orthorhombic strain. With such an assumption we expect that varying the pseudogap strength with orthorhombic strain will also change T_c, and this process will contribute to $N(p)$. Qualitatively, in this scenario we expect that at low doping $N(p)$ vanishes with orthorhombicity for reasons of symmetry, while at high doping $N(p)$ decreases because the pseudogap strength itself reduces with doping [53]. Thus, $N(p)$ is guaranteed to have an extrema at intermediate doping. Quantitatively, our theory modeling of $N(p)$ consists of the following three steps.

First, we consider the free energy involving the superconducting order parameter ϕ and the in-plane uniform strains (u_{11}, u_{22}). To simplify the discussion we first assume a system with tetragonal symmetry. The free energy has the form

$$F = \frac{1}{2}a\phi^2 + \frac{1}{2}c_{11}u_{11}^2 + \frac{1}{2}c_{22}u_{22}^2 + c_{12}u_{11}u_{22} + \lambda_1(u_{11}+u_{22})\phi^2 + \frac{1}{2}\lambda_2(u_{11}-u_{22})^2\phi^2 + \cdots, \quad (2)$$

where the ellipsis implies terms irrelevant for the current discussion. Here $a = a_0(T - T_c^0)$, where T_c^0 is the superconducting transition temperature in the absence of strain, $c_{11} = c_{22}$ and c_{12} are elastic constants in Voigt notation, and (λ_1, λ_2) are coupling constants. In an orthorhombic system we have $u_{11} = u_0/2 + \epsilon_{11}$, and $u_{22} = -u_0/2 + \epsilon_{22}$, where u_0 is the spontaneous orthorhombic strain, and $(\epsilon_{11}, \epsilon_{22})$ are strains that may develop in response to external stresses. Thus, to linear order in the induced strains ϵ_{ii} the transition temperature is

$$T_c(\epsilon_{ii}) = T_c^0 - \frac{2\lambda_1}{a_0}(\epsilon_{11}+\epsilon_{22}) - \frac{2\lambda_2}{a_0}u_0(\epsilon_{11}-\epsilon_{22}),$$

and from which we obtain

$$N = 4u_0\lambda_2/a_0. \quad (3)$$

Second, we deduce a microscopic expression for the parameter a_0. Since the superconducting transition is an instability in the particle-particle channel, we can write

$$a = 1/g - \frac{1}{k_B T}\sum_{\mathbf{k},\omega_n} f_{\mathbf{k}}^2 G_{\mathbf{k}}(i\omega_n)G_{-\mathbf{k}}(-i\omega_n), \quad (4)$$

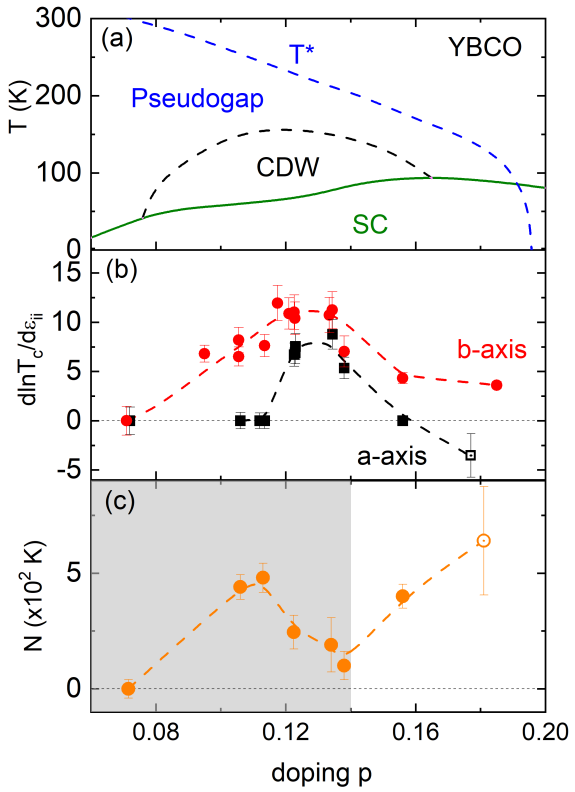

FIG. 2: a) Temperature - doping phase diagram of YBCO in zero magnetic field. Green line is the superconducting dome, black dashed line is the dome of short range CDW, blue dashed line is the pseudogap onset temperature $T^\star$. b) Doping dependence of $dT_c/d\epsilon_{11}$ (black) and $dT_c/d\epsilon_{22}$ (red), divided by T_c. c) Thermodynamic anisotropy $N = dT_c/d\epsilon_{22}-dT_c/d\epsilon_{11}$. The shaded area highlights the doping range where the anisotropy is mostly controled by the physics of the CuO_2 planes, and consequently where comparison with the theoretical model is most relevant (see text). Dashed lines are guide to the eyes. Data from this study are shown using solid symbols [52].

where g is the pairing potential, k_B is Boltzmann constant, $f_{\mathbf{k}}$ is a d-wave form factor, and $G_{\mathbf{k}}(i\omega_n)$ is the electron Green's function. We use the Yang-Zhang-Rice model [54] type of model for the Green's function

$$G^R_{\mathbf{k}}(\omega)^{-1} = \omega + i\Gamma_1 - \epsilon_{\mathbf{k}} - \frac{P^2_{\mathbf{k}}}{\omega + i\Gamma_2 + \xi_{\mathbf{k}}}, \qquad (5)$$

which has been widely used in the literature to study the low-energy properties of the pseudogap [55–62]. Here, $\epsilon_{\mathbf{k}}$ is the electron dispersion, $\xi_{\mathbf{k}} = -\omega$ defines the line along which the electron spectral function is suppressed at a given frequency, (Γ_1, Γ_2) are inverse lifetimes, and the pseudogap potential $P_{\mathbf{k}} \equiv f_{\mathbf{k}} P_0$ is assumed to have d-wave symmetry. Once the Green's function is known, the quantity a_0 follows simply from

$$a_0 = (\partial a/\partial T)_{T=T_c^0}. \qquad (6)$$

Third, we obtain a similar microscopic expression for the parameter λ_2. We consider a tetragonal system with an externally imposed orthorhombic strain $\eta \equiv u_{11} - u_{22}$. For finite η one expects mixing between A_{1g} and B_{1g} symmetries. Thus, the four-fold symmetric functions $(\epsilon_{\mathbf{k}}, \xi_{\mathbf{k}})$ develop a d-wave component, while the pseudogap potential $P_{\mathbf{k}}$ develops an s-wave component. We express these changes as $\epsilon_{\mathbf{k}} \to \tilde{\epsilon}_{\mathbf{k}} = \epsilon_{\mathbf{k}} + \alpha_1 \eta f_{\mathbf{k}}$, $\xi_{\mathbf{k}} \to \tilde{\xi}_{\mathbf{k}} = \xi_{\mathbf{k}} + \alpha_2 \eta f_{\mathbf{k}}$, and $P_{\mathbf{k}} \to \tilde{P}_{\mathbf{k}} = P_{\mathbf{k}} + \beta \eta P_0$, where (α_1, α_2) are constant energy scales and β is an important dimensionless constant capturing the change of pseudogap with *external* orthorhombic strain. From Eq. (2) we get

$$\lambda_2 = (1/2)(\partial^2 a/\partial^2 D), \qquad (7)$$

where the derivative

$$\frac{\partial}{\partial D} \equiv \alpha_1 f_{\mathbf{k}} \frac{\partial}{\partial \epsilon_{\mathbf{k}}} + \alpha_2 f_{\mathbf{k}} \frac{\partial}{\partial \xi_{\mathbf{k}}} + \beta P_0 \frac{\partial}{\partial P_{\mathbf{k}}}.$$

Following our earlier hypothesis, we chose the constants $(\alpha_1, \alpha_2, \beta)$ such that the derivative above is dominated by the last term which is the main pseudogap contribution. Thus, Eqs. (3)-(7) and the experimental input of u_0 obtained from diffraction data provide a means to compute the thermodynamic anisotropy N. The details of the particular microscopic model used and the technical steps for the computation of a_0 and λ_2 can be found in [27].

The results of the calculation are shown in Fig. 3. Our main theoretical conclusion is that, in the presence of the pseudogap, the thermodynamic anisotropy $N(p)$ (the solid line) has a maximum around $p = 0.11$ doping, as seen in the experiments. Beyond this doping the thermodynamic anisotropy decreases even though the crystalline anisotropy, namely the spontaneous orthorhombicity $u_0(p)$, increases until around $p = 0.16$. The non-monotonic behavior of $N(p)$ is a result of the presence of the pseudogap. This point is clearly demonstrated by the monotonic evolution of the open symbols in Fig. 3 which are obtained by setting the pseudogap to

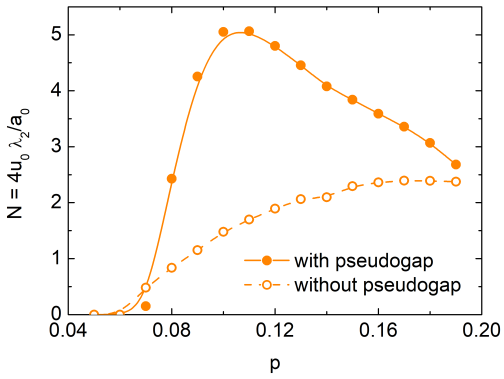

FIG. 3: Theoretical $N = 4u_0\lambda_2/a_0$ computed with $P_g \neq 0$ (full circles) and $P_g = 0$ (empty circles), using a doping dependent orthorhombicity u_0 from scattering measurements [27], and the pseudogap potential from [53]. Without pseudogap, N increases monotonically, mimicking the doping dependent orthorhombicity. The effect of the pseudogap is to produce a non-monotonic N.

zero. In other words, the doping dependence of $N(p)$ is controlled by an interplay between orthorhombicity and the pseudogap. Thus, in Fig. 3 the initial increase of $N(p)$ for $0.05 \leq p \leq 0.11$ is driven by the increase in the orthorhombicity $u_0(p)$, with the magnitude of $N(p)$ boosted by the presence of the pseudogap. While, the later decrease of $N(p)$ (the solid line) with doping beyond $p = 0.11$ is driven by a decrease of the pseudogap potential P_0 and, therefore, a decrease of $\lambda_2(p)$. The role of the pseudogap to enhance the in-plane electronic anisotropy has been also noted in an earlier dynamical mean field study [63].

In the actual experiments $N(p)$ has a minimum around $p \sim 0.14$, and it increases with further hole doping, a behavior reminiscent of electrical resistivity [1] and thermal expansion [64]. In this regime the pseudogap decreases (see Fig. 2) and our model loses significance. Simultaneously, the impact of the CuO chains, whose oxygen content increases with doping, becomes increasingly significant for the anisotropy. A second possibility is that, with increasing doping the nematic correlations become stronger [20].

To conclude, using ultrasounds on YBCO we extract $dT_c/d\epsilon_{ii}$, the variation of the superconducting transition temperature T_c with in-plane strain ϵ_{ii}. We show that the in-plane thermodynamic anisotropy $N \equiv dT_c/d\epsilon_{22} - dT_c/d\epsilon_{11}$ has an intriguing doping p dependence that does not follow that of the crystalline orthorhombicity. The reported doping dependence of N can be qualitatively accounted for by a Yang-Zhang-Rice type of phenomenological modelling of the opening of the pseudogap in the single-particle electronic properties. Our theory shows that $N(p)$ is crucially affected by the strain de-

pendence of the pseudogap potential, which makes $N(p)$ a non-monotonic function of p with a maximum around $p \sim 0.11$. Finally, an important *prediction* of our work is that, in the presence of substantial uniaxial strain, the pseudogap potential would vary significantly and, in particular, can lead to visible gap opening in the nodal region. This prediction can be tested by performing angle resolved photoemission, electronic Raman response, in-plane resistivity and Hall measurements under uniaxial strain.

We thank C. Meingast, M. Civelli, M.-H. Julien, A. Sacuto and Y. Gallais for valuable discussions. Part of this work was performed at the LNCMI, a member of the European Magnetic Field Laboratory (EMFL). Work at the LNCMI was supported by the Laboratoire d'Excellence LANEF (ANR-10-LABX-51-01), French Agence Nationale de la Recherche (ANR) grant ANR-19-CE30-0019-01 (Neptun) and EUR grant NanoX nANR-17-EURE-0009. Self-flux growth was performed at Scientific facility crystal growth in Max Planck Institute for Solid State Research, Stuttgart, Germany with the support of the technical staffs.

[1] Y. Ando *et al.* Phys. Rev. Lett. **88** 137005 (2002)
[2] Y. Sato, S. Kasahara, H. Murayama, Y. Kasahara, E.-G. Moon, T. Nishizaki, T. Loew, J. Porras, B. Keimer, T. Shibauchi and Y. Matsuda, Nat. Phys. **13**, 1074 (2017)
[3] V. Hinkov *et al.*, Science **319**, 597 (2008)
[4] L. Mangin-Thro, Y. Li, Y. Sidis, and P. Bourges, Phys. Rev. Lett. **118**, 097003 (2017)
[5] A. J. Achkar *et al.*, Science **351** 576 (2016)
[6] R. Daou *et al.*, Nature **463** 519 (2010)
[7] O. Cyr-Choiniere *et al.* Phys. Rev. B **92** 224502 (2015)
[8] M. J. Lawler *et al.*, Nature **466**, 347 (2010).
[9] Y. Zheng, *et al.*, Sci. Rep. **7**, 8059 (2017).
[10] T. Wu, *et al.*, Nat. Comm. **6**, 6438 (2015).
[11] K. Ishida *et al.,* JPSJ **89** 064707 (2020).
[12] J. Wu *et al.*, Nature **547** 432 (2017).
[13] L. Niea,, G. Tarjus, and S. A. Kivelson, Proc. Nat. Acad. Sc. (USA) **111**, 7980 (2014).
[14] E. Fradkin, S. A. Kivelson, and J. M. Tranquada, Rev. Mod. Phys. **87**, 457 (2015).
[15] C. Morice, D. Chakraborty, X. Montiel, C. Pépin, J. Phys. Condens. Matter **30**, 295601 (2018).
[16] S. Sachdev, H. D. Scammell, M. S. Scheurer, and G. Tarnopolsky, Phys. Rev. B **99**, 054516 (2019).
[17] P. P. Orth, B. Jeevanesan, R. M. Fernandes, and J. Schmalian, npj Quantum Mater. **4**, 4 (2019).
[18] E. Gull, O. Parcollet, P. Werner, and A. J. Millis, Phys. Rev. B **80**, 245102 (2009).
[19] Y. Gallais, R. M. Fernandes, I. Paul, L. Chauvière, Y. -X. Yang, M. -A. Méasson, M. Cazayous, A. Sacuto, D. Colson, and A. Forget, Phys. Rev. Lett. **111**, 267001 (2013).
[20] N. Auvray, S. Benhabib, M. Cazayous, R. D. Zhong, J. Schneeloch, G. D. Gu, A. Forget, D. Colson, I. Paul, A. Sacuto, and Y. Gallais, Nat. Comm. **10**, 5209 (2019).
[21] Kraut, O., Meingast, C., Brauchle, G., Claus, H., Erb, A., Müller-Vogt, G., and Wühl, H. Uniaxial pressure dependence of T_c of untwinned $YBa_2Cu_3O_x$ single crystals for x=6.5–7. Physica C: Superconductivity **205**, 139–146 (1993)
[22] V. Pasler, PhD thesis, Karlsruhe university (2000)
[23] J. D. Jörgensen *et al.*, Phys. Rev. B 41, 1863 (1990)
[24] H. Casalta *et al.*, Physica C 258, 321 (1996)
[25] Ch. Krüger *et al.*, Journal of Solid State Chemistry 134, 356 (1997)
[26] Liang, R., Bonn, D. A. and Hardy, W. N. Evaluation of CuO_2 plane hole doping in $YBa_2Cu_3O_{6+x}$ single crystals Physical Review B **73** 180505 (2006)
[27] See Supplementary Materials for experimental details, additional data, fitting model, error bar estimation , comparison with uniaxial pressure results
[28] Varshni, Y. P. Temperature Dependence of the Elastic Constants Phys. Rev. B **2** 3952-3958 (1970)
[29] Millis, A. J. and Rabe, K. M. Superconductivity and lattice distortions in high-T_c superconductors Phys. Rev. B **38**, 8908-8919 (1988)
[30] Lüthi, B. Physical Acoustics in the Solid State, Springer Series for Solid-State Sciences, Vol. 148 (Springer, Berlin, New York, 2005).
[31] Nohara, M.; Suzuki, T.; Maeno, Y.; Fujita, T.; Tanaka, I. and Kojima, H. Unconventional lattice stiffening in superconducting LSCO single crystals Phys. Rev. B **52** 570-580 (1995)
[32] A. Junod Physica C **162-164** 482 (1989)
[33] H. Wuhl Physica C **185-189** 482 (1991)
[34] H. Claus PhysicaC **198** 42 (1992)
[35] Loram, J.W., Luo, J., Cooper, J.R., Liang, W.Y., and Tallon, J.L. Evidence on the pseudogap and condensate from the electronic specific heat. Journal of Physics and Chemistry of Solids **62** 59–64 (2001)
[36] Marcenat, C. et al. Calorimetric determination of the magnetic phase diagram of underdoped Ortho-II YBCO single crystals. Nat. Commun. **6** 7927 (2015)
[37] C. Meingast Phys. Rev. B **41** 11299 (1990)
[38] C. Meingast Phys. Rev Lett. **67** 1634 (1991)
[39] U. Welp Phys. Rev. Lett. **69** 2130 (1992)
[40] U Welp Journal of Superconductivity **7** 159 (1994)
[41] H. A. Ludwig J. of Low Temp. Phys. **105** 1385 (1996)
[42] MarK E. Barber *et al.* preprint at arXiv:2101.02923 (2021)
[43] Ghiringhelli, G., Tacon, M.L., Minola, M., Blanco-Canosa, S., Mazzoli, C., Brookes, N.B., Luca, G.M.D., Frano, A., Hawthorn, D.G., He, F., et al. (2012). Long-Range Incommensurate Charge Fluctuations in $(Y,Nd)Ba_2Cu_3O_{6+x}$. Science **337**, 821–825.
[44] Chang, J., Blackburn, E., Holmes, A.T., Christensen, N.B., Larsen, J., Mesot, J., Liang, R., Bonn, D.A., Hardy, W.N., Watenphul, A., *et al.* Direct observation of competition between superconductivity and charge density wave order in $YBa_2Cu_3O_{6.67}$. Nat Phys **8**, 871–876 (2012).
[45] O. Cyr-Choinière Phys. Rev. B 98, 064513 (2018)
[46] I. Vinograd *et al.* Phys. Rev. B 100, 094502 (2019)
[47] H.-H. Kim *et al.* Science **362** 1040 (2018)
[48] H.-H. Kim *et al.*, Phys. Rev. Lett. **126** 037002 (2021)
[49] Forgan, E. M. *et al.* The microscopic structure of charge

density waves in underdoped $YBa_2Cu_3O_y$ revealed by X-ray diffraction. Nat. Commun. **6** 10064 (2015)
[50] R. Comin *et al.* Science (2015)
[51] D. Labat, P. Kotetes, B. M. Andersen, and I. Paul, Phys. Rev. B **101**, 144502 (2020).
[52] $dT_c/d\epsilon_{11}$ for $p = 0.18$ (empty black square, panel b) is determined using measurements of T_c under uniaxial stress [39], converted into strain dependence of T_c (see [27]). We use this value to calculate N for $p \approx 0.18$ (empty orange circle, panel c)
[53] J. Tallon and J. Loram, Physica C **349** 53 (2001).
[54] K.-Y. Yang, T. M. Rice, and F.-C. Zhang, Phys. Rev. B **73**, 174501 (2006).
[55] B. Kyung, S. S. Kancharla, D. Sénéchal, A.-M. S. Tremblay, M. Civelli, and G. Kotliar, Phys. Rev. B **73**, 165114 (2006).
[56] T. D. Stanescu and G. Kotliar, Phys. Rev. B **74**, 125110 (2006).
[57] A. Liebsch and N.-H. Tong, Phys. Rev. B **80**, 165126 (2009).
[58] S. Sakai, Y. Motome, and M. Imada, Phys. Rev. Lett. **102**, 056404 (2009).
[59] S. Sakai, M. Civelli, Y. Nomura, M. Imada, Phys. Rev. B **92**, 180503(R) (2015).
[60] W. Wu, M. S. Scheurer, S. Chatterjee, S. Sachdev, A. Georges, and M. Ferrero, Phys. Rev. X **8**, 021048 (2018).
[61] M. R. Norman, M. Randeria, H. Ding, and J. C. Campuzano, Phys. Rev. B **57**, R11093 (1998).
[62] M. R. Norman, A. Kanigel, M. Randeria, U. Chatterjee, and J. C. Campuzano, Phys. Rev. B **76**, 174501 (2007).
[63] S. Okamoto, D. Sénéchal, M. Civelli, and A. -M. S. Tremblay, Phys. Rev. B **82**, 180511(R) (2010).
[64] Peter Nagel, PhD thesis, Karlsruhe university (2001)

SUPPLEMENTARY MATERIAL FOR

Evidence for interplay between pseudogap and orthorhombicity in underdoped $YBa_2Cu_3O_y$ from ultrasound measurements

M. Frachet[1] *et al.*,
[1]LNCMI-EMFL, CNRS UPR3228, Univ. Grenoble Alpes, Univ. Toulouse, Univ. Toulouse 3, INSA-T, Grenoble and Toulouse, France

1. Experimental details

The samples used in this study are detwinned single crystals of $YBa_2Cu_3O_y$ grown from high-purity starting materials. Note that for each oxygen concentration several samples with slightly different T_c and doping were measured. In total 20 samples were studied.
Sound velocity variation $\Delta v_s/v_s$ was measured using a standard pulse-echo technique [65]. For high symmetry modes the sound velocity v_s and the elastic constant c_{ii} are related according to $\Delta v_s/v_s = \Delta c_{ii}/2c_{ii}$. We focused on the sound velocity of the longitudinal mode propagating along the b-axis (c_{22}) and along the a-axis (c_{11}). The strain is defined as $\epsilon_{ii} = \frac{l_0 - l}{l_0}$ with l_0 the initial lattice parameter.

2. Elastic constant anomaly at T_c for $p = 0.185$ and $p = 0.095$

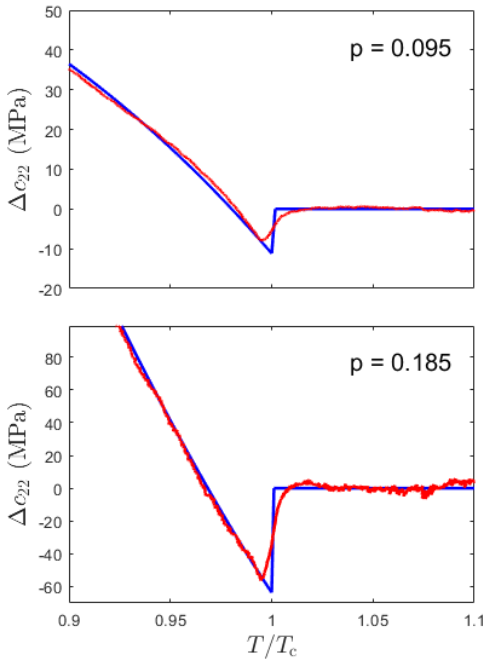

Supplementary Figure S1: Superconducting contribution to c_{22} for YBCO $p = 0.095$ (top panel) and $p = 0.185$ (bottom panel). The thermodynamic fit using Eq. S2 is shown in blue, data are shown in red.

3. Thermodynamic model used to fit the data

In order to extract $dT_c/d\epsilon_{ii}$, we estimate the magnitude of $\Delta c_{ii}(T_c)$ using an idealized mean-field second order jump fit to the data as done previously [66, 67]. The thermodynamic fit is derived from a two-fluid model of the free energy, in which

T_c and the condensation energy ϕ are functions of the strain ϵ_{ii}:

$$\Delta F = -\phi(\epsilon_{ii}) \times (1 - T^2/T_c^2(\epsilon_{ii}))^2 \tag{S1}$$

The elastic constant is obtained by calculating the second derivative of the free energy with respect to ϵ_{ii}:

$$\Delta c_{ii}(T) = -\left(\frac{d\ln T_c}{d\epsilon_{ii}}\right)^2 \frac{T\Delta C_p(T)}{V_{mol}} + AT\Delta S(T) + \frac{1}{\phi}\frac{d^2\phi}{d\epsilon_{ii}^2}\Delta F(T) \tag{S2}$$

where A is proportional to the strain derivatives of T_c and ϕ [66]. At $T = T_c$ this equation is equivalent to the Ehrenfest relationship.

4. Error bars

The error bars on $dT_c/d\epsilon_{ii}$ are estimated as follows. Most of the uncertainty comes from the value of the specific heat jump at T_c, $\Delta C_p(T_c)$. The specific heat was not measured in the samples used for this study. We relied on specific heat data from the literature. $\Delta C_p(T_c)/T_c$ are shown in figure S2 where the shaded area highlights the scattering of the data, and is used to estimate the error bar on $\Delta C_p(T_c)/T_c$.

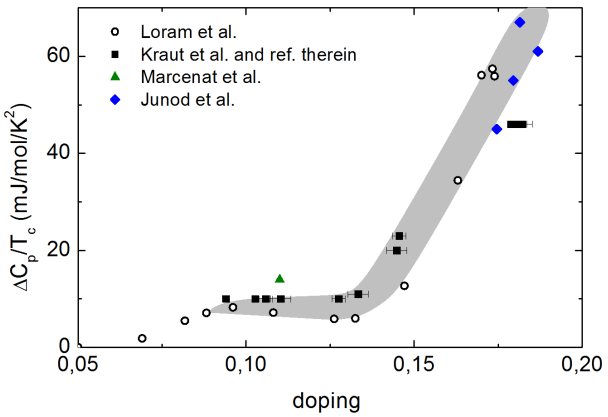

Supplementary Figure S2: Reproduction of specific heat jump at T_c ($\Delta C_p/T_c$) as a function of doping from the literature[68–72]. The error bars on $\Delta C_p/T_c$ are evaluated using the scattering of the different data set, highlighted by the gray shaded area.

Another source of error comes from the uncertainty on the absolute value of the elastic constants c_{11} and c_{22}. The pulse-echo technique used in this study allows to measure the absolute value of the sound velocity with an accuracy of a few %. This originates from the uncertainty on the sample dimension and from the fact that we used transducers with finite thickness, resulting in irregular echo shape. Comparing our data in YBCO 6.99 with data of Lei *et al.* [73] and ref. therein, we estimate an error $\Delta c_{ii}/c_{ii} \approx 6$ %. We took into account the doping dependence of c_{11} and c_{22} using a parabolic model [75]

$$c_{ii}(y) = \langle c\rangle + (y-6)^2\big(c_{ii}(y=7) - \langle c\rangle\big) \tag{S3}$$

with

$$\langle c\rangle = \frac{c_{11}(y=7) + c_{22}(y=7)}{2} \tag{S4}$$

y is the oxygen content in $YBa_2Cu_3O_y$, and we used $c_{11}(y=7) = 215$ GPa and $c_{22}(y=7) = 255$ GPa. The previous formula reflects the doping dependence of c_{ii} due to the orthorhombicity of YBCO. c_{11} and c_{22} must converge to the same value at low doping level, and are increasingly different with increasing doping. This formula results in 6 % change in c_{ii} across the doping range studied here. This doping dependence was not observed experimentally most likely because of the low accuracy of the pulse-echo method. Taken into account this doping dependence has little effect on the resulting doping dependence of $dT_c/d\epsilon_{ii}$, given the large doping dependence of the latter. Nonetheless, we took it into account for the sake of completeness of the analysis.

Other sources of error include experimental errors (variations of the amplitude of the elastic constant jump at T_c for different samples at similar doping level), uncertainties on the evaluation of the thermal phonon background which is subtracted to the data to isolate the superconducting contribution, and errors from the thermodynamic fit.

5. Comparison with uniaxial pressure results

The derivatives $dT_c/d\epsilon_{ii}$ and dT_c/dP_i are related via the formula $dT_c/d\epsilon_{ii} = \sum_j c_{ij} dT_c/dP_j$. Consequently, in order to compare our results with those from uniaxial pressure measurements we need the complete elastic tensor of YBCO. For the calculation of dT_c/dP_i we use data from Lei *et al.* [73] and ref. therein, obtained in overdoped YBCO, and we assume doping independent elastic constants. The uncertainties on the off-diagonal elastic constants are large and result in large error bars in the $dT_c/d\epsilon_{ii}$ obtained this way. In Fig.S3, we plot $dT_c/d\epsilon_{ii}$ estimated from measurements of thermal expansion [67, 77] and direct measurements under uniaxial pressure [78–80]. Values are also reported in Table S1. There is an overall agreement between all the data sets.

p (holes/Cu)	$dT_c/d\epsilon_{11}$(K)	$dT_c/d\epsilon_{22}$(K)	Ref.
0.086	170 ± 149	450 ± 168	[79]
0.094	407 ± 455	1008 ± 374	[67]
0.106	233 ± 465	961 ± 401	[67]
0.120	168 ± 275	709 ± 170	[80]
0.129	0 ± 275	626 ± 388	[79]
0.133	1068 ± 537	1548 ± 469	[67]
0.177	-320 ± 201	277 ± 217	[79]
0.182	-405 ± 324	486 ± 340	[67]

Supplementary Table S1: $dT_c/d\epsilon_{ii}$ calculated from $\sum_j c_{ij} dT_c/dP_j$ where dT_c/dP_i was measured in direct uniaxial pressure experiments [79, 80] or with thermal expansion [67]. Elastic constants value taken from [73].

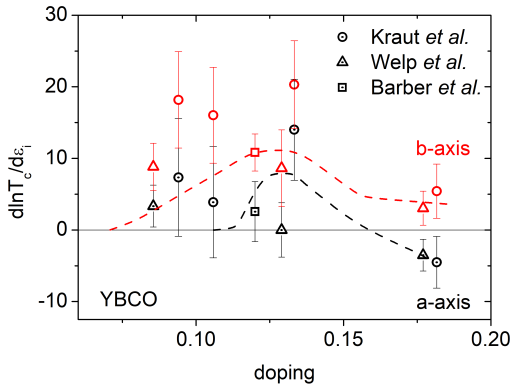

Supplementary Figure S3: Data from uniaxial pressure (triangles [79], squares [80]) and thermal expansion (circles) [67] measurements converted in uniaxial strain dependences. Red is for $dT_c/d\epsilon_{22}$ and black (with center dot) for $dT_c/d\epsilon_{11}$. The error bars are large due to the uncertainty on the elastic tensor and on the dT_c/dP_i. Dashed lines are the same as those shown in Fig. 2b of the main text.

6. Orthorhombicity

The orthorhombicity from diffraction experiments is shown in blue in Fig. S4. At low doping level, the orthorhombicity increases steadily as oxygen content in the CuO chains is increased. However, for doping levels $p > 0.15$ or so, the orthorhombicity saturates whereas the oxygen content keeps increasing.This saturation can be caused by the pressure of the oxygen ordering process in the CuO chains of YBCO [74, 75]. Increasing oxygen content results in an increase in the anisotropy of in-plane electronic transport [76] and in-plane thermal expansivities [75], even in the doping range where the orthorhombicity saturated. Assuming the sound velocity has a similar doping-dependent anisotropy as thermal expansivity, the increase of the measured N for $p > 0.15$ can be naturally explained.
For practical purposes, the anisotropy from diffraction experiments (blue dotted line in Fig. S4) is used for computing the theoretical doping dependence of N, such as shown in Fig. 4 of the main text.

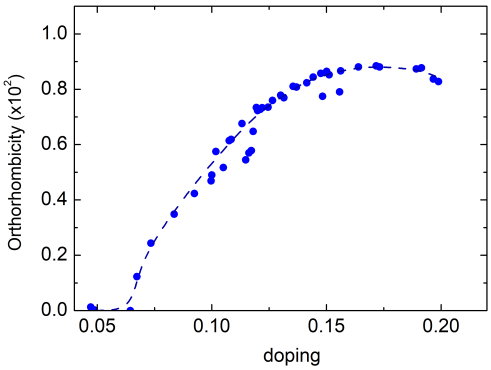

Supplementary Figure S4: Blue circles (left axis) show the orthorhombicity $u_0 = (b-a)/(b+a)$ as a function of hole doping, measured in diffraction experiments [81–83]. The blue dotted line is a guide to the eye. This dotted line is used to calculate $N \propto u_0$ (see below).

7. Theoretical details

Using Landau-Ginzburg type argument we established that the measured thermodynamic anisotropy $N \equiv dT_c/d\epsilon_{22} - dT_c/d\epsilon_{11}$ can be expressed as (see Eq. (3) of main text)

$$N = 4u_0\lambda_2/a_0.$$

In the above u_0 is the orthorhombicity, which is known experimentally. Below we provide the technical details for computing the quantities a_0 and λ_2 starting from a microscopic model. These are defined by Eqs. (6) and (7), respectively, of the main text.

Our starting point is the assumption that the low energy electrons can be described by the Green's function (see Eq. (5) of the main text)

$$G^R_{\mathbf{k}}(\omega)^{-1} = \omega + i\Gamma_1 - \epsilon_{\mathbf{k}} - \frac{P^2_{\mathbf{k}}}{\omega + i\Gamma_2 + \xi_{\mathbf{k}}}.$$

This ansatz has been widely used in the literature to capture the low energy properties of the cuprates in the pseudogap state. The above can be rewritten as

$$G^R_{\mathbf{k}}(\omega) = \frac{A_{1\mathbf{k}}}{\omega - \omega_{1\mathbf{k}}} + \frac{A_{2\mathbf{k}}}{\omega - \omega_{2\mathbf{k}}}, \tag{S5}$$

where

$$\omega_{1\mathbf{k},2\mathbf{k}} = \frac{1}{2}\left[(z_{1\mathbf{k}} + z_{2\mathbf{k}}) \pm \sqrt{(z_{1\mathbf{k}} - z_{2\mathbf{k}})^2 + 4P^2_{\mathbf{k}}}\right], \tag{S6}$$

with $z_{1\mathbf{k}} \equiv \epsilon_{\mathbf{k}} - i\Gamma_1$, $z_{2\mathbf{k}} \equiv -\xi_{\mathbf{k}} - i\Gamma_2$, and

$$A_{1\mathbf{k}} = \frac{\omega_{1\mathbf{k}} - z_{1\mathbf{k}}}{\omega_{1\mathbf{k}} - \omega_{2\mathbf{k}}}, \quad A_{2\mathbf{k}} = \frac{z_{2\mathbf{k}} - \omega_{2\mathbf{k}}}{\omega_{1\mathbf{k}} - \omega_{2\mathbf{k}}}. \tag{S7}$$

In terms of the Green's function the particle-particle susceptibility is given by

$$\chi_{pp}[\epsilon_{\mathbf{k}}, \xi_{\mathbf{k}}, P_{\mathbf{k}}] = \frac{2}{\beta V}\sum_{\mathbf{k},\omega_n}^{|\epsilon_{\mathbf{k}}|\le\Lambda} f^2_{\mathbf{k}} G_{\mathbf{k}}(i\omega_n) G_{-\mathbf{k}}(-i\omega_n), \tag{S8}$$

where β is inverse temperature, V is volume, and we assume that the Cooper pairing potential is zero above a cutoff energy scale Λ. The form factor $f_{\mathbf{k}} \equiv \cos(k_x) - \cos(k_y)$ implies that the pairing instability is in the d-wave channel. Note, χ_{pp} is a functional of the dispersions $(\epsilon_{\mathbf{k}}, \xi_{\mathbf{k}})$, and the pseudogap function $P_{\mathbf{k}}(p) = P_0(p) f_{\mathbf{k}}$. Here $P_0(p)$ is the energy scale of the pseudogap potential that varies with hole doping.

First, we discuss the details of the computation of λ_2. We assume that T^0_c, the superconducting transition temperature in the absence of external strains, is the lowest energy scale in the problem. Then, for the computation of λ_2 it is sufficient to set temperature $T = 0$. In this limit the above frequency sum can be performed analytically, and we get

$$\chi_{pp} = \frac{2}{\pi V}\sum_{\mathbf{k}}^{|\epsilon_{\mathbf{k}}|\le\Lambda} f^2_{\mathbf{k}}\left[\left(\frac{A_{1\mathbf{k}}A^*_{1\mathbf{k}}}{E_{1\mathbf{k}}} + 2X'_{\mathbf{k}}\right)\cot^{-1}\left(\frac{\gamma_{1\mathbf{k}}}{E_{1\mathbf{k}}}\right) + \left(\frac{A_{2\mathbf{k}}A^*_{2\mathbf{k}}}{E_{2\mathbf{k}}} + 2X'_{\mathbf{k}}\right)\cot^{-1}\left(\frac{\gamma_{2\mathbf{k}}}{E_{2\mathbf{k}}}\right) - X''_{\mathbf{k}}\ln\left(\frac{E^2_{2\mathbf{k}} + \gamma^2_{2\mathbf{k}}}{E^2_{1\mathbf{k}} + \gamma^2_{1\mathbf{k}}}\right)\right], \tag{S9}$$

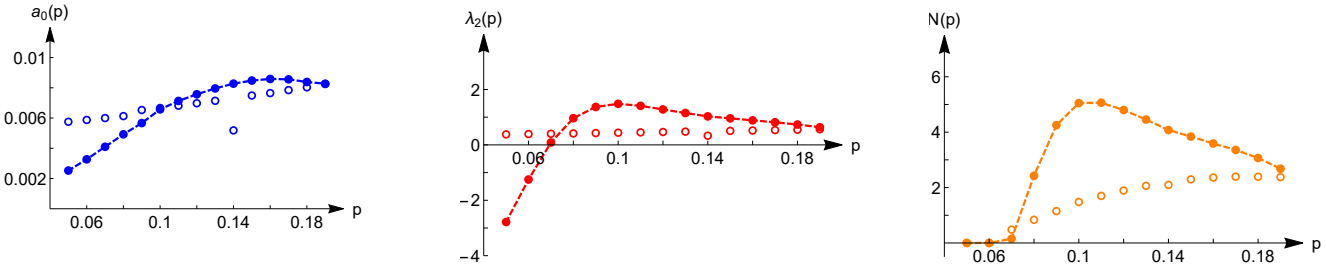

(a) (b) (c)

Supplementary Figure S5: (a, b, c) Variations of the quantities $a_0(p)$, $\lambda_2(p)$ and the thermodynamic anisotropy $N(p)$ as functions of hole doping, respectively. Filled symbols are with finite pseudogap, and open symbols are calculations with the pseudogap potential set to zero. The theoretical model correctly captures the appearance of a maximum in $N(p)$, as seen experimentally. This feature disappears, and $N(p)$ is a monotonic function of p when the pseudogap is set to zero.

where $E_{1\mathbf{k}/2\mathbf{k}}$ and $\gamma_{1\mathbf{k}/2\mathbf{k}}$ are real quantities that are defined by $\omega_{1\mathbf{k}/2\mathbf{k}} \equiv E_{1\mathbf{k}/2\mathbf{k}} - i\gamma_{1\mathbf{k}/2\mathbf{k}}$, and the complex quantity $X_{\mathbf{k}} = X'_{\mathbf{k}} + iX''_{\mathbf{k}} \equiv A_{1\mathbf{k}}A_{2\mathbf{k}}/[E_{1\mathbf{k}} + E_{2\mathbf{k}} + i(\gamma_{2\mathbf{k}} - \gamma_{1\mathbf{k}})]$. In the presence of a finite external orthorhombic strain η the quantities $(\epsilon_{\mathbf{k}}, \xi_{\mathbf{k}}, P_{\mathbf{k}})$ transform to $(\tilde{\epsilon}_{\mathbf{k}}, \tilde{\xi}_{\mathbf{k}}, \tilde{P}_{\mathbf{k}})$, where $\tilde{\epsilon}_{\mathbf{k}} = \epsilon_{\mathbf{k}} + \alpha_1\eta f_{\mathbf{k}}$, $\tilde{\xi}_{\mathbf{k}} = \xi_{\mathbf{k}} + \alpha_2\eta f_{\mathbf{k}}$, and $\tilde{P}_{\mathbf{k}} = P_{\mathbf{k}} + \beta\eta P_0$. From Eq. (7) of the main text we get $\lambda_2 = -1/2(\partial^2\chi_{pp}/\partial^2\eta)_{\eta=0}$. This implies that

$$\lambda_2 = -\frac{1}{\pi V}\sum_{\mathbf{k}}^{|\epsilon_{\mathbf{k}}|\leq\Lambda} f_{\mathbf{k}}^2\left(\alpha_1 f_{\mathbf{k}}\frac{\partial}{\partial\epsilon_{\mathbf{k}}} + \alpha_2 f_{\mathbf{k}}\frac{\partial}{\partial\xi_{\mathbf{k}}} + \beta P_0\frac{\partial}{\partial P_{\mathbf{k}}}\right)^2 L_{\mathbf{k}}, \tag{S10}$$

where $L_{\mathbf{k}}$ denotes the quantity within $[\cdots]$ in Eq. (S9). In the above equation it is straightforward to take the derivatives and then perform the momentum sum numerically. This leads to the evaluation of $\lambda_2(p)$ as a function of hole doping p.
Next, we discuss the details of the computation of $a_0 = -(\partial\chi_{pp}/\partial T)_{T=T_c^0}$. In terms of the Green's function this can be written as

$$a_0 = \frac{2}{V}\sum_{\mathbf{k}}^{|\epsilon_{\mathbf{k}}|\leq\Lambda} f_{\mathbf{k}}^2\,\mathrm{Im}\int_{-\infty}^{\infty}\frac{d\omega}{2\pi}G_{\mathbf{k}}^R(\omega)G_{\mathbf{k}}^A(-\omega)\frac{\omega}{2T^2\cosh^2(\omega/(2T))}. \tag{S11}$$

The thermal factor ensures that the ω-integral contributes only for $\omega \lesssim T = T_c^0$. Since T_c^0 is the lowest energy scale, the Green's functions can be expanded in powers of the frequency. This is equivalent to an expansion in powers of $T_c^0/\max[\Gamma_1, P_0]$. We keep the first non-zero term, and we get

$$a_0 = \frac{2T_c^0}{3\pi V}\sum_{\mathbf{k}}^{|\epsilon_{\mathbf{k}}|\leq\Lambda} f_{\mathbf{k}}^2\left[\frac{A_{1\mathbf{k}}A_{1\mathbf{k}}^*\gamma_{1\mathbf{k}}}{(E_{1\mathbf{k}}^2+\gamma_{1\mathbf{k}}^2)^2} + \frac{A_{2\mathbf{k}}A_{2\mathbf{k}}^*\gamma_{2\mathbf{k}}}{(E_{2\mathbf{k}}^2+\gamma_{2\mathbf{k}}^2)^2} + \mathrm{Im}\left\{\frac{A_{1\mathbf{k}}A_{2\mathbf{k}}^*}{(E_{1\mathbf{k}}-i\gamma_{1\mathbf{k}})(E_{2\mathbf{k}}+i\gamma_{2\mathbf{k}})}\left(\frac{1}{E_{1\mathbf{k}}-i\gamma_{1\mathbf{k}}} - \frac{1}{E_{2\mathbf{k}}+i\gamma_{2\mathbf{k}}}\right)\right\}\right]. \tag{S12}$$

It is simple to perform the momentum sum numerically, which leads to $a_0(p)$ as a function of hole doping p.
We compute a_0, λ_2 and the thermodynamic anisotropy $N(p)$ using the following model and parameters. The dispersions are taken as

$$\epsilon_{\mathbf{k}} = -2t(\cos(kx)+\cos(ky)) + 4t'\cos(kx)\cos(ky) - 2t''(\cos(2kx)+\cos(2ky)) - \mu, \tag{S13a}$$
$$\xi_{\mathbf{k}} = -2t(\cos(kx)+\cos(ky)), \tag{S13b}$$

with $t = 1$, $t' = 0.3t$, $t'' = 0.2t$. The damping factors are set to $\Gamma_1 = 0.1t$, and $\Gamma_2 = 0.01t$. The pseudogap potential is set to $P_0(p) = P_g(1 - p/0.2)$, with $P_g = 0.3t$. Thus, $P_0(p)$ is assumed to decrease linearly with hole doping, and disappearing at $p = 0.2$. Next, we take the energy scales $\alpha_1 = \alpha_2 = 0.5t$, and the dimensionless parameter $\beta = -10$, and the overall energy cutoff $\Lambda = 0.3t$. For the computation of $N(p)$ we use the experimental values of the spontaneous orthorhombicity $u_0(p)$ of $YBa_2Cu_3O_y$.
The results of the calculation are shown in Fig. S5. Our main conclusion is that in the presence of the pseudogap the thermodynamic anisotropy $N(p)$ indeed has a maximum around $p = 0.11$ doping, see the evolution of the filled symbols in Fig. S5(c). Beyond this doping the thermodynamic anisotropy decreases even though the crystalline anisotropy, namely the spontaneous orthorhombicity $u_0(p)$ increases until $p = 0.18$. The non-monotonic behavior of $N(p)$ is a result of the presence of the pseudogap. This point is clearly demonstrated by the monotonic evolution of the open symbols in Fig. S5(c) which are obtained by setting the pseudogap to zero.
The decrease of $N(p)$ for $p > 0.1$ in our calculation is the result of the following two features. First, the increase of $a_0(p)$ in this doping range. This is due to the fact that the pseudogap decreases with increasing doping and, therefore, there is more

phase space for the contribution of the low energy electrons to the susceptibility χ_{pp} and to its temperature dependence. In general, we expect that susceptibilities are less temperature dependent in the presence of gaps. Second, the decrease in the magnitude of $\lambda_2(p)$ over the same doping range. This feature is the result of our assumption that the pseudogap potential varies significantly in the presence of an external uniaxial strain. Thus, around $p \approx 0.11$ the contribution to λ_2 is dominated by the term $(\partial/\partial P_{\mathbf{k}})^2$ in Eq. (S10) in our model. On the other hand, by definition, at $p = 0.2$ this contribution [and also from terms involving $(\partial/\partial\xi_{\mathbf{k}})$] vanishes. In other words, an important *prediction* of our work is that, in the presence of substantial uniaxial strain the pseudogap potential would vary significantly and, in particular, can lead to visible gap opening in the nodal region. This prediction can be tested by performing spectroscopy such as angle resolved photoemission and electronic Raman response under uniaxial strain.

In the actual experiments $N(p)$ has a minimum around $p \sim 0.14$ and then increases with further hole doping. We think this regime is dominated by the contribution of the anisotropy coming from the CuO chains, rather than the electrons of the copper-oxygen planes. Consequently, this increase is not captured in our theoretical modeling.

SUPPLEMENTARY REFERENCES

[65] Lüthi, B. Physical Acoustics in the Solid State, Springer Series for Solid-State Sciences, Vol. 148 (Springer, Berlin, New York, 2005).

[66] Nohara, M.; Suzuki, T.; Maeno, Y.; Fujita, T.; Tanaka, I. and Kojima, H. Unconventional lattice stiffening in superconducting LSCO single crystals Phys. Rev. B **52** 570-580 (1995)

[67] Kraut, O., Meingast, C., Brauchle, G., Claus, H., Erb, A., Müller-Vogt, G., and Wühl, H. Uniaxial pressure dependence of T_c of untwinned $YBa_2Cu_3O_x$ single crystals for x=6.5–7. Physica C: Superconductivity **205**, 139–146 (1993)

[68] A. Junod Physica C **162-164** 482 (1989)

[69] H. Wuhl Physica C **185-189** 482 (1991)

[70] H. Claus PhysicaC **198** 42 (1992)

[71] Loram, J.W., Luo, J., Cooper, J.R., Liang, W.Y., and Tallon, J.L. Evidence on the pseudogap and condensate from the electronic specific heat. Journal of Physics and Chemistry of Solids **62** 59–64 (2001)

[72] Marcenat, C. et al. Calorimetric determination of the magnetic phase diagram of underdoped Ortho-II YBCO single crystals. Nat. Commun. **6** 7927 (2015).

[73] Lei, M.; Sarrao, J. L.; Visscher, W. M.; Bell, T. M.; Thompson, J. D.; Migliori, A.; Welp, U. W. and Veal, B. W. Elastic constants of a monocrystal of superconducting $YBa_2Cu_3O_7$ Phys. Rev. B **47** 6154-6156 (1993)

[74] P. Nagel *et al.*, Phys. Rev. Lett. **85** 2376 (2000)

[75] Peter Nagel, PhD thesis, Kalrsruhe university (2001)

[76] Y. Ando *et al.* Phys. Rev. Lett. **88** 137005 (2002)

[77] C. Meingast Phys. Rev Lett. **67** 1634 (1991)

[78] U. Welp Phys. Rev. Lett. **69** 2130 (1992)

[79] U Welp Journal of Superconductivity **7** 159 (1994)

[80] MarK E. Barber *et al.* preprint at arXiv:2101.02923 (2021)

[81] J. D. Jörgensen *et al.*, Phys. Rev. B 41, 1863 (1990)

[82] H. Casalta *et al.*, Physica C 258, 321 (1996)

[83] Ch. Krüger *et al.*, Journal of Solid State Chemistry 134, 356 (1997)